J. Fluid Mech. (2017), *vol.* 831, R2, doi:10.1017/jfm.2017.679

JFM RAPIDS
journals.cambridge.org/rapids

How we compute *N* matters to estimates of mixing in stratified flows

Robert S. Arthur[1,†], **Subhas K. Venayagamoorthy**[2,3], **Jeffrey R. Koseff**[3] **and Oliver B. Fringer**[3]

[1]Lawrence Livermore National Laboratory, Livermore, CA 94550, USA

[2]Department of Civil and Environmental Engineering, Colorado State University, Fort Collins, CO 80523, USA

[3]The Bob and Norma Street Environmental Fluid Mechanics Laboratory, Department of Civil and Environmental Engineering, Stanford University, Stanford, CA 94305, USA

(Received 15 June 2017; revised 29 August 2017; accepted 18 September 2017)

Most commonly used models for turbulent mixing in the ocean rely on a background stratification against which turbulence must work to stir the fluid. While this background stratification is typically well defined in idealized numerical models, it is more difficult to capture in observations. Here, a potential discrepancy in ocean mixing estimates due to the chosen calculation of the background stratification is explored using direct numerical simulation data of breaking internal waves on slopes. Two different methods for computing the buoyancy frequency N, one based on a three-dimensionally sorted density field (often used in numerical models) and the other based on locally sorted vertical density profiles (often used in the field), are used to quantify the effect of N on turbulence quantities. It is shown that how N is calculated changes not only the flux Richardson number R_f, which is often used to parameterize turbulent mixing, but also the turbulence activity number or the Gibson number Gi, leading to potential errors in estimates of the mixing efficiency using Gi-based parameterizations.

Key words: internal waves, stratified turbulence, turbulent mixing

1. Introduction

Diapycnal mixing, or the molecular diffusion of density across isopycnal surfaces, is a primary control on the ocean stratification (Munk & Wunsch 1998; Wunsch & Ferrari 2004). Turbulent stirring enhances this mixing by deforming isopycnal surfaces, creating both sharper density gradients and a greater surface area over which molecular diffusion can occur. Turbulent stirring is reversible, and represents an

† Email address for correspondence: arthur7@llnl.gov

exchange between turbulent kinetic energy and available potential energy. Diapycnal mixing, however, is irreversible; it represents a sink of turbulent kinetic energy into the background potential energy of the fluid. Due to difficulties associated with measuring the turbulent fluxes that lead to diapycnal mixing in the ocean (see, e.g., Ivey, Winters & Koseff 2008; Venayagamoorthy & Koseff 2016), a great deal of work has gone into estimating mixing using indirect methods. Such methods typically rely on directly measured quantities such as the turbulent kinetic energy dissipation rate ϵ or the temperature variance dissipation rate χ.

As outlined by Ivey *et al.* (2008), there are two common approaches for indirectly estimating turbulent mixing in the ocean. The first is the model of Osborn (1980), which is based on measurements of ϵ, and approximates the turbulent diffusivity of density with

$$K_\rho = \left(\frac{R_f}{1-R_f}\right)\frac{\epsilon}{N^2} = \varGamma\frac{\epsilon}{N^2}, \tag{1.1}$$

where N is the buoyancy frequency. The model also depends on the flux Richardson number $R_f = \mathcal{B}/\mathcal{P}$, where $\mathcal{B}$ is the turbulent buoyancy flux and $\mathcal{P}$ is the rate of production of turbulent kinetic energy. Following Ivey & Imberger (1991), the flux Richardson number is sometimes defined more generally as $R_f = \mathcal{B}/(\mathcal{B}+\epsilon)$. The term $\varGamma = R_f/(1-R_f)$ is referred to as the mixing efficiency and represents the ratio of the turbulent buoyancy flux to the turbulent dissipation. The second commonly used mixing model is that of Osborn & Cox (1972), which is based on measurements of $\chi = 2\kappa_\theta\overline{|\boldsymbol{\nabla}\theta'|^2}$, where θ' is the temperature fluctuation from the background temperature $\overline{\theta}$ and κ_θ is the molecular diffusivity of heat. Using this model, the turbulent diffusivity of heat is given by

$$K_\theta = 3\kappa_\theta\frac{\overline{\left(\dfrac{\partial\theta'}{\partial n}\right)^2}}{\left(\dfrac{\partial\overline{\theta}}{\partial n}\right)^2}, \tag{1.2}$$

where n is normal to isothermal surfaces, but in the field is always assumed to be the vertical direction z (Ivey *et al.* 2008).

Based on their derivations from the turbulent kinetic energy equation and the temperature variance equation respectively, both the Osborn & Cox (1972) model and the Osborn (1980) model rely on a fundamental assumption that the flow is steady and homogeneous. However, this assumption is often violated in the ocean due to the intermittent (unsteady) and patchy (inhomogeneous) nature of ocean turbulence (Ivey *et al.* 2008). Many studies have therefore related mixing to certain non-dimensional numbers, such as the turbulent Froude number and turbulent Reynolds number, that describe the state of the turbulence that leads to mixing (e.g. Ivey & Imberger 1991; Mater & Venayagamoorthy 2014*a*).

Additionally, both the Osborn & Cox (1972) model and the Osborn (1980) model rely on a more implicit assumption which has received less attention in the literature: the stratification (N in Osborn 1980; $\partial\overline{\theta}/\partial n$ in Osborn & Cox 1972) is assumed to represent the background gradient against which turbulence must work to stir the fluid. The background stratification is typically well defined in idealized numerical models, which have been used extensively to study turbulent mixing. For example, it can be held constant (e.g., Shih *et al.* 2005) or it can be obtained through an adiabatic rearrangement of the full three-dimensional density field (Winters *et al.* 1995; Scotti & White 2014). However, the appropriate background stratification is much less obvious in the ocean, and even to some extent in the laboratory (e.g. Hult, Troy & Koseff 2011).

Due to practical limitations in the ocean, turbulence data are almost always gathered using vertical-profiling instruments. Thus, when the Osborn & Cox (1972) and Osborn (1980) models are used in the field, the background stratification is estimated through adiabatic rearrangement, or sorting, of one-dimensional vertical density profiles. This practice began with the study of Thorpe (1977), continued with Dillon (1982), and is still very common today (see, e.g., Thorpe 2005; Ivey *et al.* 2008). Due to the intermittent patchy nature of turbulence in the ocean, it is unclear how well this estimated background stratification represents the true stratification against which turbulence is working. Any differences between the background stratification calculated using this methodology and the true background stratification will translate to errors in estimates of turbulent mixing.

In this study, the discrepancy in estimates of turbulent mixing that arises from the chosen calculation of the background stratification is quantified in the context of breaking internal waves on slopes. Particular attention is paid to the flux Richardson number R_f, which must be determined in order to estimate mixing from measurements of ϵ and N using the Osborn (1980) model. While Osborn (1980) originally assumed a constant $R_f \approx 0.17$, many parameterizations have been developed to estimate R_f based on the state of the turbulence (e.g. Ivey & Imberger 1991; Shih *et al.* 2005; Bouffard & Boegman 2013). Due to the difficulties in calculating R_f in unsteady inhomogeneous turbulence in the field, these parameterizations are generally based on the results of idealized laboratory experiments and direct numerical simulations (DNS). Several field studies that have measured the turbulent buoyancy flux directly (e.g. Davis & Monismith 2011; Walter *et al.* 2014) have shown good agreement with existing parameterizations. The study of Mater & Venayagamoorthy (2014*b*) provides a thorough summary of the current state of R_f parameterizations in the literature. However, the existence of a 'universal' parameterization for R_f remains an open question.

The effect of the background stratification on the resulting mixing calculation is quantified using the DNS dataset of Arthur, Koseff & Fringer (2017). As highlighted in figure 1, breaking internal waves on slopes are an inherently unsteady inhomogeneous flow, and are thus a useful case study for calculating and interpreting R_f. By varying the calculation of N, it is shown that the chosen method can affect not only R_f, but also the values of the non-dimensional parameters upon which R_f depends.

2. Methods

The DNS dataset of Arthur *et al.* (2017) includes results from eight breaking wave cases with varying interface thickness (and thus varying stratification), but with similar incoming wave properties. From these data, turbulent dissipation and irreversible mixing quantities are calculated as follows. Turbulent dissipation is defined as

$$\epsilon_k^t = 2\nu \overline{S'_{ij} S'_{ij}}, \tag{2.1}$$

where ν is the kinematic viscosity and $S'_{ij} = ((\partial u'_i/\partial x_j) + (\partial u'_j/\partial x_i))/2$ is the turbulent rate-of-strain tensor. Irreversible turbulent mixing is defined generally as

$$\epsilon_p^t = \kappa \frac{\overline{|\nabla b'|^2}}{N^2}, \tag{2.2}$$

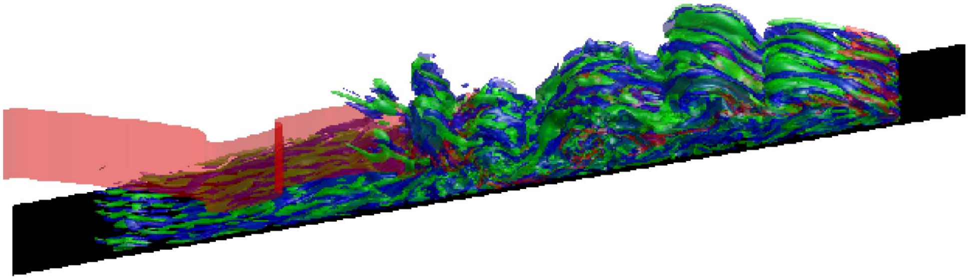

FIGURE 1. A three-dimensional view of the turbulent flow field during breaking for an internal wave with intermediate interface thickness (case 5 in Arthur *et al.* 2017). Isosurfaces of the reference density $\rho=\rho_0$ (red), positive streamwise vorticity $\Omega_1/\omega=37$ (blue) and negative streamwise vorticity $\Omega_1/\omega=-37$ (green) are shown, where ω is the frequency of the incoming wave.

where $b=g(\rho-\rho_0)/\rho_0$ is the buoyancy and κ is the molecular diffusivity of density. In (2.1) and (2.2), the overbar denotes a lateral average (in the x_2 direction), while the prime denotes a departure from that average. Calculations of ϵ_k^t and ϵ_p^t are therefore functions of x_1, x_3 and t.

The buoyancy frequency N is calculated in two ways in order to study its effect on quantifying turbulent energetics. First, following Scotti & White (2014), $N=N^*$, where N^* is the buoyancy frequency of the background density profile ρ^*. The background density profile represents the lowest possible potential energy state of the system if it were to be adiabatically rearranged (Winters *et al.* 1995), and is obtained numerically by sorting the full three-dimensional density field ρ into a one-dimensional vertical density profile ρ^* at each time step. The sorting algorithm may be thought of as a 'filling up' of the domain with the fluid from each individual grid cell without any mixing in order to create a density field that varies only in the vertical, making ρ^* and N^* functions of x_3 and t only. Changes in the background density profile (and, thus, the background potential energy) can only occur due to molecular diffusion, and are therefore irreversible. When irreversible mixing is calculated using $N=N^*$ in (2.2), it is denoted ϵ_p^{t*}. When calculating ϵ_p^{t*}, since the term $\overline{|\nabla b'|^2}$ is laterally averaged, the numerator is a function of x_1 and x_3. The buoyancy frequency in the denominator, N^*, is therefore computed by interpolating the value of x_3^* such that $\rho^*(x_3^*)=\overline{\rho}(x_1,x_3)$, and then using the value of N^* at that value of x_3^*.

The ability to calculate the background buoyancy frequency N^* using the three-dimensionally sorted density field represents an advantage of DNS that is not possible using observational data. Instead, N is often determined by sorting a vertical density profile through a turbulent patch. As in Smyth, Moum & Caldwell (2001) and Mater, Schaad & Venayagamoorthy (2013), virtual profiles can be taken through a DNS domain in order to mimic calculations that would be made with observational data. An alternative definition is therefore $N=\hat{N}^*$, where $\hat{N}^*=\sqrt{-(g/\rho_0)\partial\hat{\overline{\rho}}^*/\partial x_3}$ and $\hat{\overline{\rho}}^*$ represents an adiabatic rearrangement of the laterally averaged vertical density profile at each x_1 grid point in the DNS domain at each time step. Thus, $\hat{\overline{\rho}}^*$ and $\hat{N}^*$ are functions of x_1, x_3 and t. When irreversible mixing is calculated using $N=\hat{N}^*$ in (2.2), it is denoted $\hat{\epsilon}_p^{t*}$.

Using the definitions in (2.1) and (2.2), an irreversible flux Richardson number can be calculated generally as (e.g. Scotti & White 2014)

$$R_f = \epsilon_p^t / (\epsilon_p^t + \epsilon_k^t). \tag{2.3}$$

This is a preferable measure of R_f to the previous definition in § 1, which can include reversible turbulent buoyancy fluxes and is therefore not fully irreversible (Venayagamoorthy & Koseff 2016). Here, the irreversible flux Richardson number calculated with ϵ_p^{t*} (using $N = N^*$ in (2.2)) is denoted R_f^*, and that calculated with $\hat{\epsilon}_p^{t*}$ (using $N = \hat{N}^*$ in (2.2)) is denoted $\hat{R}_f^*$.

In order to examine the effect of stratification on the irreversible flux Richardson number, and how this changes for different methods of calculating N, turbulence data are examined as a function of the Gibson number (Monismith *et al.* 2017),

$$Gi = \epsilon_k^t / \nu N^2. \tag{2.4}$$

Also known as the buoyancy Reynolds number Re_b or the turbulence activity number, Gi quantifies the scale separation between the smallest turbulent eddies that feel stratification and the Kolmogorov scale. The functional relationship between R_f and Gi has been calculated in the field (e.g. Davis & Monismith 2011; Walter *et al.* 2014), in the laboratory (e.g. Barry 2002) and in DNS (e.g. Shih *et al.* 2005). In what follows, Gi values calculated with $N = N^*$ are denoted Gi^*, while those calculated with $N = \hat{N}^*$ are denoted $\hat{Gi}^*$.

3. Results

Due to lateral averaging in (2.1) and (2.2), the turbulence dataset derived from the three-dimensional DNS data of Arthur *et al.* (2017) is two-dimensional (i.e. a function of x_1, x_3 and t). In the analysis that follows, the area-weighted frequency of occurrence f is calculated relative to several turbulence quantities. Because the computational grid used in Arthur *et al.* (2017) is non-uniform, area weighting is based on the (x_1, x_3) area of each grid cell. The frequency f can be thought of as the probability of finding a data point within a given bin of the chosen turbulence quantity.

3.1. *How turbulence quantities depend on the computation of N*

Since Gi is itself a function of the buoyancy frequency N, it is first instructive to see how it varies with the method of computing N. A direct comparison may be made using a two-dimensional histogram of $f(Gi^*, \hat{Gi}^*)$ (figure 2*a*), which shows that $\hat{Gi}^*$ is generally greater than Gi^*, especially for turbulent regions where $Gi > 1$. Because the calculation of ϵ_k^t is independent of the method used to compute N, this indicates that $\hat{N}^*$ is generally less than N^*. The two-dimensional histogram of $f(\epsilon_p^{t*}, \hat{\epsilon}_p^{t*})$ (figure 2*b*) provides further evidence that $\hat{N}^*$ underestimates N^*. The term $\hat{\epsilon}_p^{t*}$ is generally larger than ϵ_p^{t*}, especially for larger mixing values (ϵ_p^t greater than roughly 1×10^{-7} m^2 s^{-3} in figure 2*b*). The observed differences in ϵ_p^t lead to differences in the flux Richardson number R_f (figure 2*c*): $\hat{R}_f^*$ is, overall, slightly larger than R_f^*, as expected from the trend in ϵ_p^t. Most notably, for R_f^* less than roughly 0.1, a region of increased $\hat{R}_f^*$ extends up to roughly 0.6, indicating large overestimates when lateral averaging and vertical sorting are used. It should be noted that R_f quantities in figure 2 are limited to turbulent regions where $Gi > 1$.

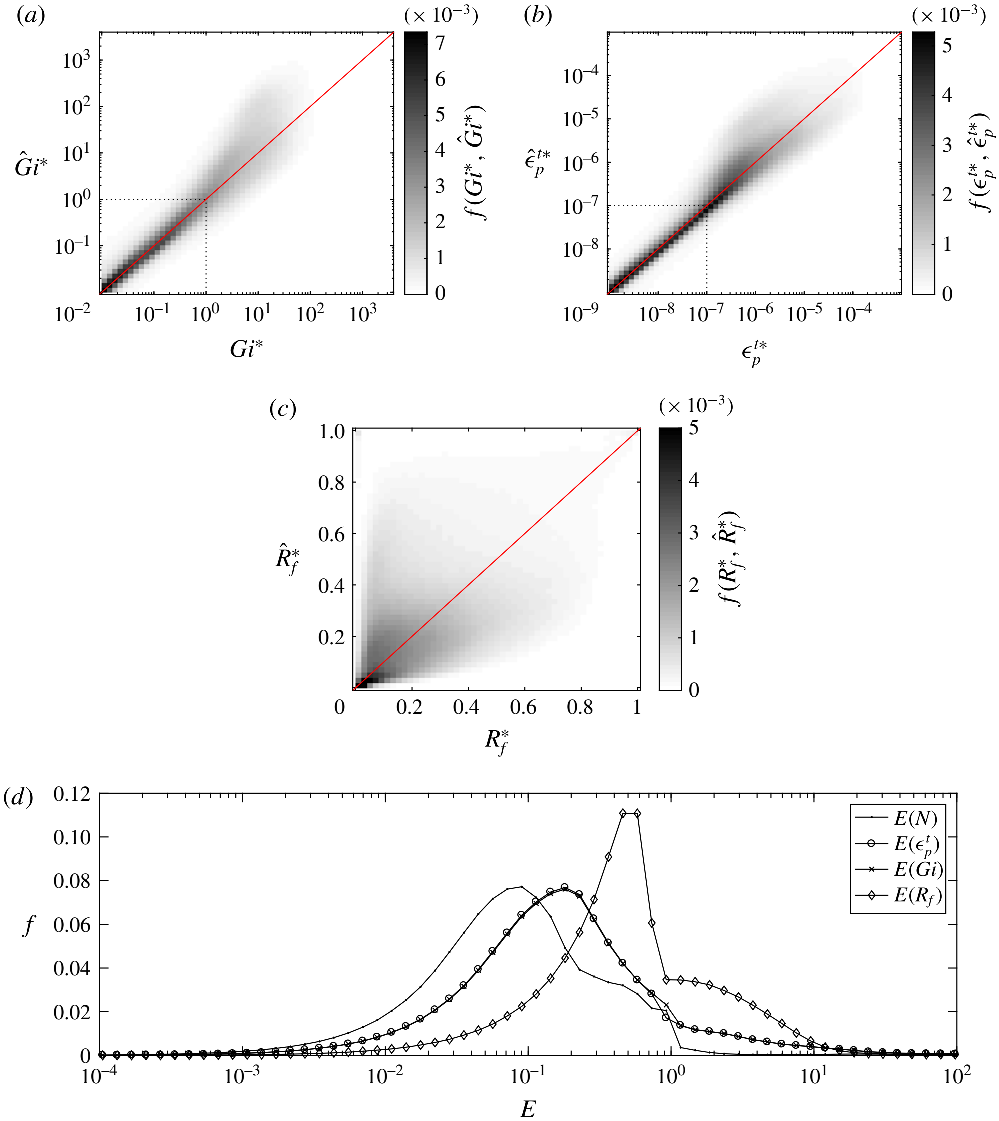

FIGURE 2. (a) Two-dimensional histogram of $f(Gi^*, \hat{Gi}^*)$. (b) Two-dimensional histogram of $f(\epsilon_p^{t*}, \hat{\epsilon}_p^{t*})$. Here, ϵ_p^t is shown in units of m^2 s^{-3}. (c) Two-dimensional histogram of $f(R_f^*, \hat{R}_f^*)$. The R_f calculations are limited to turbulent regions where $Gi > 1$. (d) Histogram of the error E in calculations of N, ϵ_p^t, Gi and R_f.

If the N value calculated from the three-dimensionally sorted density field is taken to be the true value, then the error caused by calculating N using lateral averaging and vertical sorting can be defined as

$$E(\phi) = \frac{|\hat{\phi}^* - \phi^*|}{\phi^*}, \tag{3.1}$$

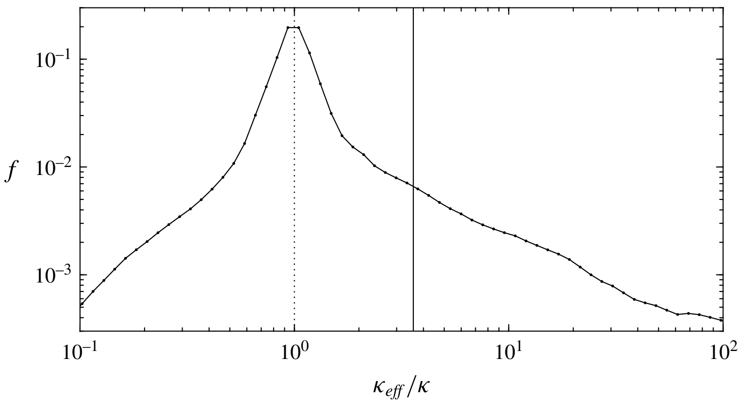

FIGURE 3. Histogram of the effective mixing rate κ_{eff} due to lateral averaging and vertical sorting. The vertical dotted line shows the true value of $\kappa = 1 \times 10^{-6}\ \mathrm{m^2\ s^{-1}}$ (Arthur *et al.* (2017) use a Prandtl number $Pr = \nu/\kappa = 1$). The vertical solid line shows the mean value of $\kappa_{eff}/\kappa = 3.6$.

where ϕ is a turbulence quantity. The histogram in figure 2(*d*) shows that $E(N)$ is often $O(10^{-1})$, and can be as large as $O(1)$. It should be noted that, as discussed above, $\hat{N}^*$ is generally less than N^*; thus, generally, $\hat{N}^* - N^* < 0$. However, the absolute value in (3.1) guarantees that $E > 0$, allowing it to be plotted on a log scale in figure 2(*d*). The error in N translates to errors in ϵ_p^t, Gi and R_f as large as $O(10)$. The terms $E(\epsilon_p^t)$ and $E(Gi)$ are nearly identical, as they are both proportional to $1/N^2$.

For the breaking wave scenarios considered here, lateral averaging and vertical sorting of density profiles unphysically smooth out variability in N, leading to mixing estimates that are larger than the true mixing values. The variability in N is better captured by full three-dimensional sorting, resulting in a more accurate measure of mixing. The additional (artificial) mixing that results from the use of $\hat{N}^*$ instead of N^* can be quantified using an effective mixing coefficient κ_{eff}, defined with

$$\hat{\epsilon}_p^{t*} = \kappa \frac{\overline{|\nabla b'|^2}}{(\hat{N}^*)^2} = \kappa_{eff} \frac{\overline{|\nabla b'|^2}}{(N^*)^2}, \tag{3.2}$$

which implies

$$\kappa_{eff} = \kappa \left(\frac{N^*}{\hat{N}^*} \right)^2. \tag{3.3}$$

The effective mixing rate κ_{eff} is clearly skewed towards values larger than the true mixing rate κ, and is, on average, 3.6 times larger than κ (figure 3).

3.2. *The flux Richardson number R_f as a function of Gi*

The method of computing N has a strong effect on the functional relationship between R_f and Gi, which is often used to parameterize mixing in the ocean. Here, R_f is calculated as a weighted mean in bins of Gi (figure 4*a*). As in the calculation of f (described at the beginning of this section), area weighting is used to account for the non-uniform grid in the simulations of Arthur *et al.* (2017). Thus, larger (smaller) grid

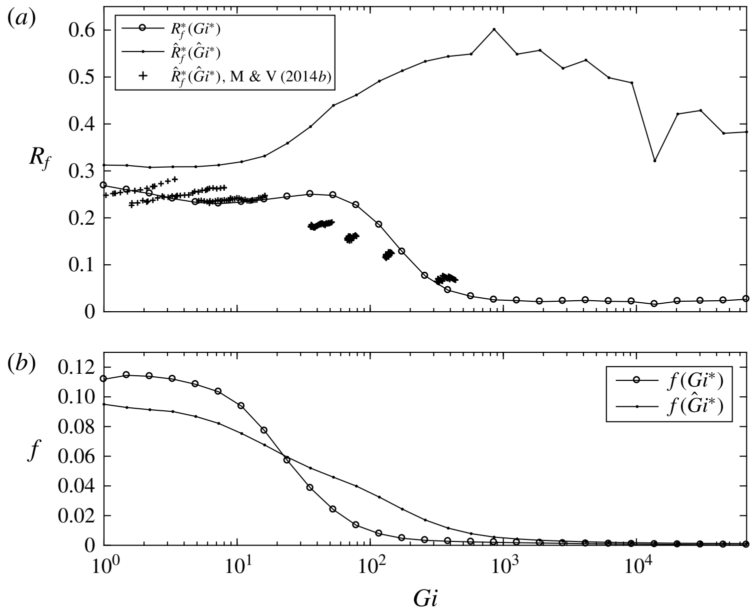

FIGURE 4. (*a*) Comparison of mean R_f^* as a function of Gi^* with mean $\hat{R}_f^*$ as a function of $\hat{Gi}^*$. The $\hat{R}_f^*$ calculation of Mater & Venayagamoorthy (2014*b*) using the data of Shih *et al.* (2005) is included as well. (*b*) Histograms of Gi^* and $\hat{Gi}^*$.

cells, which take up a larger (smaller) portion of the computational domain, contribute more (less) to the mean value of R_f. To show the spread of the data in terms of the Gibson number, f is also calculated in each Gi bin (figure 4*b*). Due to computational restrictions on Gi associated with the DNS, many of the data have relatively low (non-turbulent) values of $Gi < 1$. Since these values imply laminar flow, they are omitted in figure 4. It should be noted that calculations of R_f for larger values of Gi are based on a small subset of the data (figure 4*b*), probably explaining the wiggles in the $\hat{R}_f^*$ curve.

The term $\hat{R}_f^*$, which reaches a peak of nearly 0.6 for $\hat{Gi}^* \approx 10^3$, is generally larger than R_f^*, which has maximum values between 0.2 and 0.3 for $Gi^* < 10^2$. For $Gi^* > 10^2$, a sharp drop in the mixing efficiency occurs and R_f^* approaches 0. A similar result was found for R_f by Shih *et al.* (2005), Walter *et al.* (2014) and others; see figure 12 in Walter *et al.* (2014). Because $\hat{Gi}^*$ is generally larger than Gi^*, the decline of $\hat{R}_f^*$ for large values of $\hat{Gi}^*$ occurs at a larger value of $\hat{Gi}^*$ (approximately $\hat{Gi}^* = 10^3$).

The large discrepancies that arise in R_f when lateral averaging and vertical sorting are used on unsteady inhomogeneous breaking wave data emphasize the potential effect of N on mixing estimates in the ocean. If $Gi = 10^2$, local vertical sorting causes R_f to be overestimated by roughly a factor of 2. This increases to a factor of roughly 10 when $Gi \geqslant 10^3$. In contrast, the $\hat{R}_f^*(\hat{Gi}^*)$ calculations of Mater & Venayagamoorthy (2014*b*) using the stratified shear flow data of Shih *et al.* (2005) generally follow the present $R_f^*(Gi^*)$ curve, but depart substantially from the present $\hat{R}_f^*(\hat{Gi}^*)$ curve. This is probably due to the homogeneous nature of the turbulence studied by Shih *et al.* (2005), which could allow local vertical sorting to achieve a more accurate measure of the true background stratification. In the inhomogeneous flow studied here, $\hat{N}^*$ varies spatially, and may therefore be a less appropriate measure of N.

4. Conclusion

Two different methods of computing the buoyancy frequency N, one based on a three-dimensionally sorted density field and the other based on laterally averaged and vertically sorted density profiles, were used to calculate turbulent mixing quantities. For the breaking internal wave events considered here, the method of lateral averaging and vertical sorting ($\hat{N}^*$) generally leads to a smaller value of the buoyancy frequency relative to full three-dimensional sorting (N^*). Because N represents the background stratification against which turbulence must work to stir the fluid, reduced values of $\hat{N}^*$ lead to overestimates of mixing relative to those calculated with N^*. This, in turn, changes the functional relationship between the flux Richardson number R_f and the turbulence activity number Gi, which is commonly used to estimate mixing. These results have implications for how existing parameterizations of mixing in the ocean are used: the method of calculating N not only affects R_f, but also adds some uncertainty to its estimation using parameters, such as Gi, that also depend on N.

Acknowledgements

R.S.A. gratefully acknowledges the support of the Stanford Graduate Fellowship. R.S.A. and O.B.F. gratefully acknowledge the support of ONR grants N00014-08-1-0904 and N00014-16-1-2256 (scientific officers Dr C. Linwood Vincent, Dr T. Paluszkiewicz and Dr S. Harper). We gratefully acknowledge the US Army Research Laboratory DoD Supercomputing Resource Center for computer time on Pershing and Excalibur, and especially thank the diligent staff at the HPC Help Desk for their support. We also thank O. Murray of ONR for ensuring our access to these resources. Finally, we are grateful to two anonymous referees for their thoughtful reviews of the manuscript. A portion of this work was prepared by LLNL under Contract DE-AC52-07NA27344.

References

Arthur, R. S., Koseff, J. R. & Fringer, O. B. 2017 Local versus volume-integrated turbulence and mixing in breaking internal waves on slopes. *J. Fluid Mech.* **815**, 169–198.

Barry, M. E. 2002 Mixing in stratified turbulence. PhD thesis, University of Western Australia, Centre for Water Research.

Bouffard, D. & Boegman, L. 2013 A diapycnal diffusivity model for stratified environmental flows. *Dyn. Atmos. Oceans* **61**, 14–34.

Davis, K. A. & Monismith, S. G. 2011 The modification of bottom boundary layer turbulence and mixing by internal waves shoaling on a barrier reef. *J. Phys. Oceanogr.* **41** (11), 2223–2241.

Dillon, T. M. 1982 Vertical overturns: a comparison of Thorpe and Ozmidov length scales. *J. Geophys. Res.* **87** (C12), 9601–9613.

Hult, E. L., Troy, C. D. & Koseff, J. R. 2011 The mixing efficiency of interfacial waves breaking at a ridge: 2. Local mixing processes. *J. Geophys. Res.* **116**, C02004.

Ivey, G. N. & Imberger, J. 1991 On the nature of turbulence in a stratified fluid. Part I: the energetics of mixing. *J. Phys. Oceanogr.* **21** (5), 650–658.

Ivey, G. N., Winters, K. B. & Koseff, J. R. 2008 Density stratification, turbulence, but how much mixing? *Annu. Rev. Fluid Mech.* **40**, 169–184.

MATER, B. D., SCHAAD, S. M. & VENAYAGAMOORTHY, S. K. 2013 Relevance of the Thorpe length scale in stably stratified turbulence. *Phys. Fluids* **25**, 076604.

MATER, B. D. & VENAYAGAMOORTHY, S. K. 2014*a* The quest for an unambiguous parameterization of mixing efficiency in stably stratified geophysical flows. *Geophys. Res. Lett.* **41** (13), 4646–4653.

MATER, B. D. & VENAYAGAMOORTHY, S. K. 2014*b* A unifying framework for parameterizing stably stratified shear-flow turbulence. *Phys. Fluids* **26** (3), 036601.

MONISMITH, S. G., KOSEFF, J. R., WALTER, R. K., SQUIBB, M., PAWLAK, G., DAVIS, K. A. & DUNCKLEY, J. 2017 Buoyancy fluxes in stratified flows: observations and parameterizations. *J. Phys. Oceanogr.* (submitted).

MUNK, W. & WUNSCH, C. 1998 Abyssal recipes II: energetics of tidal and wind mixing. *Deep Sea Res.* **45** (12), 1977–2010.

OSBORN, T. R. 1980 Estimates of the local rate of vertical diffusion from dissipation measurements. *J. Phys. Oceanogr.* **10** (1), 83–89.

OSBORN, T. R. & COX, C. S. 1972 Oceanic fine structure. *Geophys. Fluid Dyn.* **3** (1), 321–345.

SCOTTI, A. & WHITE, B. 2014 Diagnosing mixing in stratified turbulent flows with a locally defined available potential energy. *J. Fluid Mech.* **740**, 114–135.

SHIH, L. H., KOSEFF, J. R., IVEY, G. N. & FERZIGER, J. H. 2005 Parameterization of turbulent fluxes and scales using homogeneous sheared stably stratified turbulence simulations. *J. Fluid Mech.* **525**, 193–214.

SMYTH, W. D., MOUM, J. N. & CALDWELL, D. R. 2001 The efficiency of mixing in turbulent patches: inferences from direct simulations and microstructure observations. *J. Phys. Oceanogr.* **31** (8), 1969–1992.

THORPE, S. A. 1977 Turbulence and mixing in a Scottish loch. *Phil. Trans. R. Soc. Lond.* **286** (1334), 125–181.

THORPE, S. A. 2005 *The Turbulent Ocean*. Cambridge University Press.

VENAYAGAMOORTHY, S. K. & KOSEFF, J. R. 2016 On the flux Richardson number in stably stratified turbulence. *J. Fluid Mech.* **798**, R1.

WALTER, R. K., SQUIBB, M. E., WOODSON, C. B., KOSEFF, J. R. & MONISMITH, S. G. 2014 Stratified turbulence in the nearshore coastal ocean: dynamics and evolution in the presence of internal bores. *J. Geophys. Res.* **119** (12), 8709–8730.

WINTERS, K. B., LOMBARD, P. N., RILEY, J. J. & D'ASARO, E. A. 1995 Available potential energy and mixing in density-stratified fluids. *J. Fluid Mech.* **289**, 115–128.

WUNSCH, C. & FERRARI, R. 2004 Vertical mixing, energy, and the general circulation of the oceans. *Annu. Rev. Fluid Mech.* **36**, 281–314.